Controllable Nanofabrication of Aggregate-like Nanoparticle Substrates and Evaluation for Surface-Enhanced Raman Spectroscopy

Sabrina M. Wells,[†] Scott D. Retterer,[‡] Jenny M. Oran,[†] and Michael J. Sepaniak[†,*]

[†]University of Tennessee, Knoxville, Tennessee 37996-1600 and [‡]Center for Nanophase Materials Sciences, Oak Ridge National Laboratory, Oak Ridge, Tennessee 37831

ABSTRACT The development of new and better substrates is a major focus of research aimed at improving the analytical capabilities of surface-enhanced Raman spectroscopy (SERS). Perhaps the most common type of SERS substrate, one consistently exhibiting large enhancements, is simple colloidal gold or silver nanoparticles in the 10—150 nm size range. The colloidal systems that are used most for ultrasensitive detection are generally aggregated clusters that possess "hot spot(s)" within some of the aggregates. A significant limitation of these synthetic substrates is that the "hot" aggregates are extremely difficult to create consistently or predict. Electron beam lithography (EBL) along with combinatorial spectral mapping can be used to overcome this limitation. Our previous work, and that of other researchers, invokes the special capabilities of EBL to design and fabricate periodic, highly ordered nanoparticle arrays for SERS. Building on this work, EBL, in conjunction with ancillary fabrication steps, can be used to create complex patterns that mimic random aggregates. These aggregates, unlike those created by colloidal deposition methods, *can be uniquely reproduced* within the resolution limits of EBL. In the work reported herein, we use a unique approach to create substrates containing a large number of randomly generated cells with different morphologies that are arrayed on silicon wafers. Instead of isolated metal nanoparticles, these structures resemble the aggregates of colloid. By spectral mapping, we investigate the SERS activity of the combinatorial arrays of cells using probe analytes. Two general categories of shapes are randomly designed in different sizes and densities into several hundred different 5 μm square cells. Following fabrication, it is shown that a SERS performance contrast of more than a factor of 44 is achieved among these cells and that the best performing cells can be cloned into uniformly high performing macropatterns of lithographically defined nanoaggregates (LDNAs). In this manner, extended LDNA surfaces with uniform 5×10^8 enhancement factors are created. Furthermore, the LDNAs can be further dissected and studied in an effort to increase the SERS enhancement per unit geometric substrate area.

KEYWORDS: surface-enhanced Raman spectroscopy · electron beam lithography · nanoparticle aggregates · nanofabrication · microscopy

Surface-enhanced Raman scattering (SERS) is a valuable analytical phenomenon that can result in a dramatic increase in Raman signal from molecules that have been sorbed onto or are in the vicinity of nanometer-sized metallic particles. There are two accepted mechanisms, chemical and electromagnetic, that are generally recognized as being responsible for the observation of the SERS effect.[1,2] Chemical enhancement mechanisms are dependent upon both analyte molecules adsorbed to the SERS substrate surface and the nature of the metal surface itself, in some cases creating a charge transfer intermediate state to increase Raman signal.[3]

Electromagnetic enhancement is more general in nature and is typically not critically dependent upon the analyte used. It can be seen in SERS when substrates are made of roughened metal surfaces or nanoparticles, typically gold, silver, or copper, that have features smaller than the wavelength of light being used.[4−6] When electromagnetic radiation impinges on the metal composing the SERS substrate, conduction band electrons undergo oscillations of frequency equal to that of the incident light. These oscillating electrons produce surface plasmons at/near the metal surface.[7] The resulting secondary electric field adds to the incident field. Thus, localized surface plasmons have the ability to enhance the electromagnetic field in the area near the nanoparticles composing the substrate, leading to greater Raman signal enhancement for analytes located therein. Similarly, the Raman scatter can be amplified by the substrate. The SERS effect is highly dependent upon nanoparticle shape and structure as it relates to the excitation wavelength and the dielectric properties of the medium.[8−10] As a result, recent research[11−13] has focused on taking advantage of the electromagnetic enhancement mechanism of SERS by engineering substrates with both random and controlled morphologies that can be used to tune the observed surface plasmon resonance to suit the experiment.

Perhaps the most common type of SERS substrate, one that consistently

*Address correspondence to msepaniak@utk.edu.

Received for review August 26, 2009 and accepted November 6, 2009.

Published online November 13, 2009.
10.1021/nn9010939

yields large signal enhancement, is simple colloidal gold or silver nanoparticles having the size range of 10−150 nm.[14,15] Usually, these are formed by the reduction of metal salts, for example, the reduction of silver nitrate with sodium citrate. In some cases, the reduction is accomplished in a more careful fashion to create cubes, rods, or triangular structures.[16] The colloidal systems that are most often used for single molecule or otherwise ultrasensitive detection are usually aggregated clusters that possess some "hot spot(s)" within certain aggregates. Research has shown "hot" aggregates can contain as few as two to six[15] tightly packed particles and be as large as greater than 20 particles.[17] Much research has been done using colloidal substrates to support the finding that nanoparticle density plays a role in Raman signal enhancement.[17−21] In one study by Khan *et al.*, the effects of aggregate size/nanoparticle density on surface-enhanced resonance Raman scattering (SERRS) signal were examined.[17] Ag colloid solution was evenly distributed across the surface of a TEM grid, and SERRS data were collected and correlated with TEM images. The results showed that, as nanoparticle density increased, SERRS activity increased. Regions of the grids that contained large aggregates showed the most intense SERRS signal, while regions with few particles were the least intense.[17] Another study by Camden *et al.* focused on the correlation between nanoparticle structures known to yield single molecule SERS, wherein several active aggregates were identified.[22] The results showed that hot spots likely occur at particle−particle intersections. A focus was made at studying a simple dual particle aggregate composed of a hemispherically capped rod and a sphere with a T-shape that yielded single molecule sensitivity.[22] While well-designed, random morphology substrates may lead to improved SERS enhancement, it is difficult to synthetically reproduce the nanoparticle aggregates that have been found to yield large SERS signal. One alternative to colloid is metal island film substrates.[23] The advantages of this type of substrate over colloid-based substrates include better reproducibility from spot to spot and ease of fabrication. However, these substrates have yet to generate the signal enhancements of the best performing colloidal systems.

Previous work in our group has demonstrated electron beam lithography (EBL) techniques for the definition and fabrication of nanostructured SERS substrates.[24−26] With EBL, the morphology of the SERS-active substrate can be controlled since the nanoparticles composing the substrate are chosen and laid out using computer-aided design software.[13,24−27] Also, EBL remains an important technique for fabricating uniform, reproducible substrates. Recently, we found that substrates made of ordered arrays of ellipses having aspect ratios of 300:300 and 300:250 nm gave better SERS enhancement than smaller, prolate ellipses (6:1 to 6:4).[26] We have also performed research with synthetically produced, random-shaped aggregated colloid and colloid shaped as cubes that have yielded good SERS enhancement, as well.[28] Along those lines, our focus herein is to combine the two approaches to substrate creation and fabricate combinatorial sets of SERS substrates composed of random patterns that can be *spectrally mapped and reproduced* based on their demonstrated enhancement.

To this end, we borrow from the biomedical concepts of combinatorial chemistry and cloning and demonstrate a novel EBL-reactive ion etching (RIE) approach to the combinatorial fabrication of SERS substrates. The substrates are arranged in 10 × 10 matrices composed of randomly different 5 × 5 μm cells of lithographic defined nanoaggregates (LDNAs) and inspected for SERS activity using benzenethiol (BT) as a test compound. We combine the randomness of colloidal aggregate substrates with the ability of the EBL system to reproduce substrate morphology by designing arrays containing aggregates made up of different shapes ranging in size from approximately 75 to 650 nm. Herein, we describe the process we used to create these LDNAs, as well as the combinatorial approach to determine the best performing aggregates. Experiments were also completed to examine reproducibility of both the aggregates, in addition to the SERS signals they produce. Finally, an experiment was used to inspect the ability of our LDNAs to be cloned over large areas while remaining uniform, intense SERS-active in the process.

RESULTS AND DISCUSSION

Spectral Mapping of Initial 50 × 50 μm Aggregate Arrays. EBL patterns were made from randomly arranged, computer-generated arrays of differing nanoparticle shapes. An array in this work is defined as the individual particles that are laid down onto the computer template. These arrayed shapes formed 5 × 5 μm cells, containing either (i) various shapes (stars, crescent moons, *etc.*) or (ii) eight different circles and ellipses, each of which is of assorted sizes totaling different coverage areas (see Table 1 for details). The cells were formed into 5 × 5 μm squares to approximate the laser spot size. Circles/ellipses were chosen to mimic the nanoparticle shapes in the hot aggregates that form *via* colloid reduction (although more disk-like than true synthetic colloids).[15,17] The various shapes were chosen to produce structures with sharper features. However, as seen in Figure 1, the nanofabrication processes tend to round-out the sharper features. These arrayed cells form the overall 50 × 50 μm patterns (a 10 × 10 matrix that contains 100 morphologically different cells) that are surveyed for SERS signals in these experiments.

In order to determine whether an original aggregate array contained areas of substantial enhance-

TABLE 1. General Morphological Data on the 8 Different Types of Tested Matrices

cell description	particle size (long dimension)	percent coverage area
larger size, higher dense various[a] shape pattern	200–650 nm	55%
larger size, less dense various shape pattern	200–650 nm	30%
smaller size, less dense various shape pattern	100–300 nm	30%
smaller size, middle density various shape pattern	100–300 nm	40%
smaller size, higher density various shape pattern	100–300 nm	55%
least dense circle/ellipse pattern	75–150 nm	15%
middle density circle/ellipse pattern	75–150 nm	25%
higher density circle/ellipse pattern	75–150 nm	35%

[a]Various shapes include circles, squares, stars, and crescents (see Figure 1 and Table 2.

TABLE 2. Results of Combinatorial-like SERS Signal Surveys of the 8 Different Types of Tested Matrices

Cell Description	CAD Appearance	Signals Highest	Signals Lowest
Larger size, various shape pattern		11196 10441 8703	766 435 976
Larger size, less dense various shape pattern		16757 4623 4732	504 727 841
Small size, less dense various shape pattern		10488 7690 8332	1512 1557 1643
Small size, middle density various shape pattern		6583 7182 6583	1438 1244 1418
Small size, highest density various shape pattern		5677 3586 4127	508 629 625
Least dense circle/ellipse pattern		22295 13610 12254	2226 2266 2164
Middle density circle/ellipse pattern	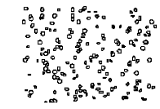	13644 10066 8980	1278 1392 1527
Highest density circle/ellipse pattern	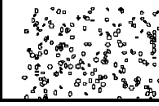	20055 19524 11668	1058 1196 1272

ment, the array was spectrally mapped and the SERS signals were obtained from the self-assembled monolayer (SAM) of benzenethiol (BT).[29,30] Twenty-five nanometers of Ag was deposited onto the different patterns at a rate of 1 Å/s. It was determined that depositing a layer of SiO_2 on the wafer prior to depositing the Ag, thereby altering the dielectric properties of the substrate, substantially improved signals.[31] Initial experiments showed that 20 nm of SiO_2 was optimum for dielectric aspects without appreciably distorting the sharp features of the EBL. In every initial 50 × 50 μm pattern, the best and worst performing of the 100 individual 5 × 5 μm cells were determined. Each individual analysis was then compared with other trials using the same parameters, including the substrate pattern type. In general, there were individual cells, or regions of cells, giving consistently high signals in each of the initial trials. Figure 2 shows the analysis of the least dense circle/ellipse pattern with a corresponding hot region in the lower right corner of the substrate. While the two hot areas seem to be in the same overall region, it is difficult to determine from the full 50 × 50 μm pattern spectral mapping experiment whether the two hot cells are identical. This is due to instrument limitations, in particular, not being able to start the rastering analysis in exactly the same spot for each trial. To obviate this limitation, we use an additional, more confined, spectral mapping experiment to pinpoint the hottest cell(s). The process is discussed in the following section.

It is also obvious from looking at Figure 2 that no discernible signal occurs outside of the 50 × 50 μm pattern. As shown, the "hot" region was not only located in the same area in both trials but the signals were almost identical. Strong performing cells were generally determined from the magnitudes of the 1056 and 1575 cm^{-1} bands. There are small relative differences in spectral features, as some minor bands are stronger in certain cells than others, presumably due to the random nature of the substrates or

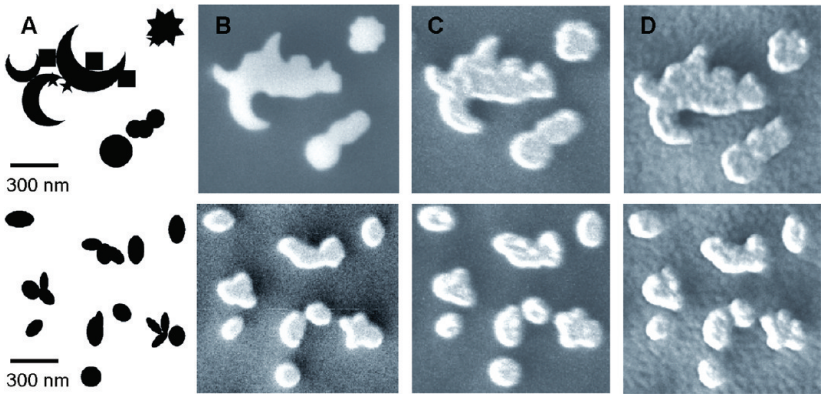

Figure 1. Images of (A) CAD of a various shape pattern (above) and circle/ellipse pattern (below) and SEMs of (B) EBL patterns following 250 nm deep RIE, (C) EBL patterns after deposition of 20 nm of SiO_2, and (D) deposition of 40 nm of Ag.

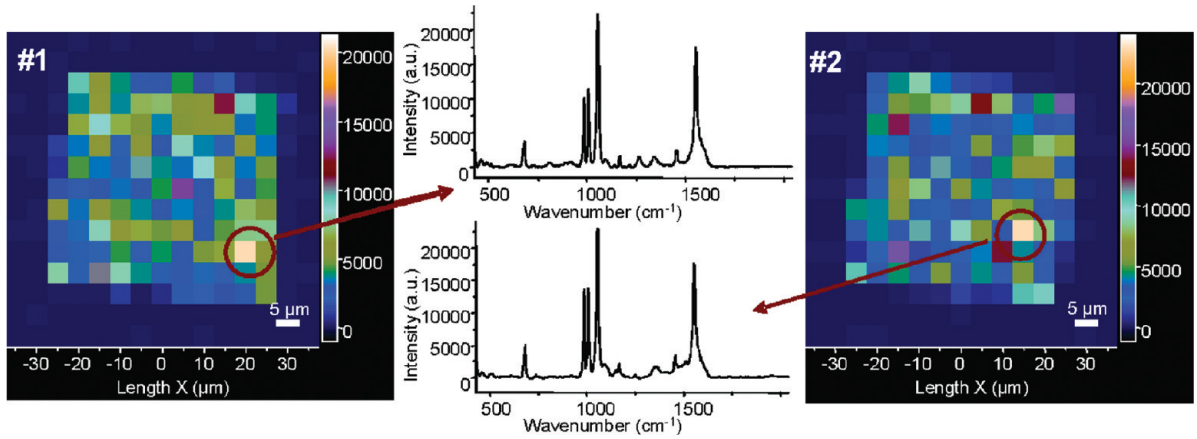

Figure 2. Combinatorial-like SERS signal survey of two 50 × 50 μm patterns of the least dense circle ellipse type of pattern. The spectra of BT for the apparent best 5 × 5 μm cells are shown.

trace impurities. In this case, the signal for the single best cell in each pattern was roughly 5 times stronger than the average signal for the entire pattern and over 10 times higher than the lower performing cells. This showed that a hot region was present in the original pattern, as well as present in each of the low-density circle/ellipse patterns tested.

This general procedure for determining hot regions was followed for all pattern types presented in Table 1. Through analysis, it was determined that the circle/ellipse patterns had an overall higher signal than the various shape patterns. Counterintuitively, those patterns with lower overall surface area performed better than those with greater area. Table 2 shows a portion of the CAD for the best cell of each pattern type, as well as the top and bottom three performing cells' signal heights at the 1056 cm^{-1} band. As illustrated in the table, the highest to lowest signals range by more than a factor of 44 in signal height. There is clearly a wide range in signals in even the same pattern. This can be attributed to the fact that the structures are random in nature. As such, some of the cells could be much "hotter" than any other part of the pattern. Therefore, determining the best performing cells in a given pattern is paramount to potentially creating reproducible structures with overall uniform strong enhancement. The process for doing so is addressed in the next section.

The circle/ellipse patterns consistently gave signal at a higher intensity than the various shape patterns. Also, the lower density patterns had better performing hot spots than the higher density substrates. The overall best performing substrate, the low density circle/ellipse pattern, had only approximately 15% coverage of each 5 × 5 μm cell. Previous EBL substrate work from our group indicated that the substrates with denser surface coverage had higher overall enhancement.[24−26] However, the prior work did not involve RIE to create pillars of Si and subsequently the creation of a layer of SiO_2. We suspect that the continuous layer of 25 nm Ag over the SiO_2 may be a factor, and experiments are planned to investigate this possibility. Note that Chumanov and co-workers have observed interesting coupling between continuous metal films and plasmonic particles.[32,33]

Determination of Best Cell. After initial analysis, it was determined that the pattern types of focus for further inquiry would include the larger size, less dense various shape pattern, and the low-density circle/ellipse pattern. They each gave a large signal, while also having hot regions located in the same general area of the 50 × 50 μm pattern for each initial trial. To determine which of the 5 × 5 μm cells was actually giving the large signal, we conducted a more confined spectral mapping experiment. To pinpoint the hot cell, a 3 × 3 cell matrix of the suspected hot cell region was created. This small 15 × 15 μm pattern helped determine the correct hot cell due to its small size and ease of reproducibility. Since there are only nine potential cells, the possibility of accidentally misdiagnosing which of the cells is giving the greatest signal is minimized. When looking at the cells in the original 50 × 50 μm pattern, there is a chance for the best region's signal to be obscured with the surrounding cells based solely on size of the substrate and limitations of the Raman instrument. As shown in Figure 3A,B, the 9 cell array confirms that the hottest point is in the same place as seen in the original array.

After determining the best individual cell, the entity was then broken into quartered sections, each 2.5 × 2.5 μm. By splitting the hot cell into individual parts, we can determine if there is uniform signal throughout the overall cell or if just a part of the whole is responsible for the majority of signal intensity. As seen in Figure 3C, the quartered sections yielded quite different signals. This shows that the individual aggregates are capable of giving signal enhancement large enough to affect the overall signal of the entire, larger cell. Further-

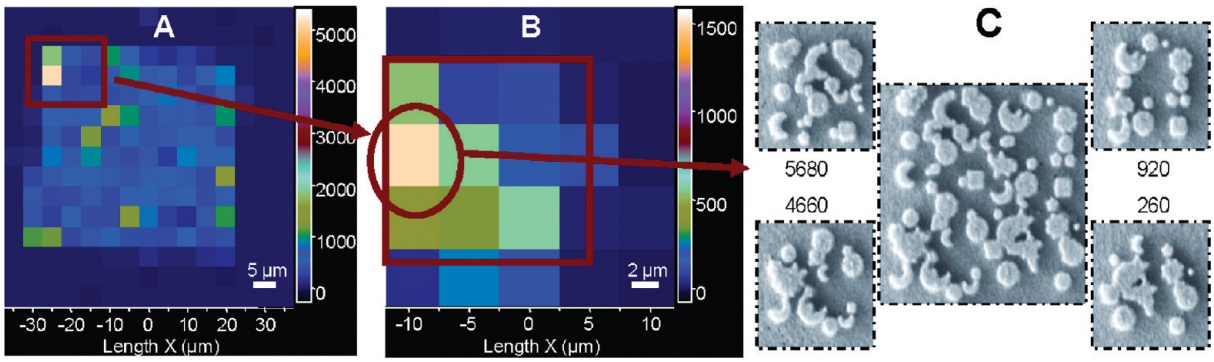

Figure 3. Combinatorial-like SERS signal survey (BT analyte) of (A) 10 × 10 cell orignal matrix, (B) a 3 × 3 cell matrix containing an apparent good cell, and (C) subdividing the good cell (SEMs and SERS signal heights from 2.5 μm square quarters); focusing on discovering good performing morphologies.

more, as the SEM images show, the EBL process is capable of creating aggregates repeatedly that are similar in nature. Each of the four corners of the original bears a close resemblance to the quartered aggregate corresponding to it.

Reproducibly Cloned Arrays. Once the top performing cell had been identified, the next step was to show that the EBL process can be used to reproducibly clone arrays of similar cells, both in appearance and performance. The top performing cell out of the low-density, circle/ellipse patterns and a modest performing cell out of the larger size, various shape pattern were selected, and a relatively large 120 × 120 μm square pattern was cloned with the best performing aggregate forming the shape of a "T" in the center. Figure 4A shows an optical image taken by our Raman instrument of what the array looks like. The pattern was then analyzed by raster mapping as done in the previous trials. Figure 4B shows the actual mapping of the cloned cell T pattern substrate. As shown, the inner part of the T seems to be uniform in signal while the outer part also seems to be a uniform color, indicating similar signal intensity. After analysis, the inner part of the pattern had an average signal band area of over 97 000 at 1056 cm^{-1} with an RSD of slightly less than 30%. The outer region had an average signal area of only 23 000 at the same band with an RSD of approximately 31%. In general, a modestly performing cell tended to yield somewhat higher signals when cloned into larger areas than when it exists as a unique cell in a diverse morphology array.

This particular pattern shows several advantages of the EBL process for SERS substrate fabrication. First is the ability to create reproducible aggregates that give uniform signal. Even though there are some uncertainties associated with enhancement factor (EF) calculations,[34] it still remains one of the ways to evaluate the SERS activity of a substrate or portion of a substrate. With this in mind, we attempted to calculate the EF for the inner part of the T region. A common procedure[35] that employs eq 1 for the SERS EF calculation was used:

$$\mathrm{EF}(1575\ \mathrm{cm}^{-1}) = \left(\frac{N_{\mathrm{vol}} I_{\mathrm{surf}}}{N_{\mathrm{surf}} I_{\mathrm{vol}}}\right) \qquad (1)$$

wherein I_{vol} and I_{surf} were the signal areas under the 1575 cm^{-1} peaks for neat BT (Raman standard) and a SAM of BT (SERS), respectively.

Knowing the laser spot size of our 50× microscope objective (~5 μm) and using the average area covered by the individual cell (15%), we calculated the total surface area of the nanoparticles and multiplied it by the known packing density of BT (6.8 × 10^{14} molecules/cm^2).[36,37] This yielded the maximum surface number density (N_{surf}) of the adsorbed molecules that lead to the SERS signal. Neat BT was used as a Raman standard in a glass capillary. The volume of the area in question was found to be 29.5 nL. Using the density of BT (1.073 g/mL) in the neat BT calculation, the number density (N_{vol}) was found to be 1.74 × 10^{14} molecules. With the above information, the average EF for the inner part of the T was calculated to be 3 × 10^8 with several cells giving enhancement of 5 × 10^8.

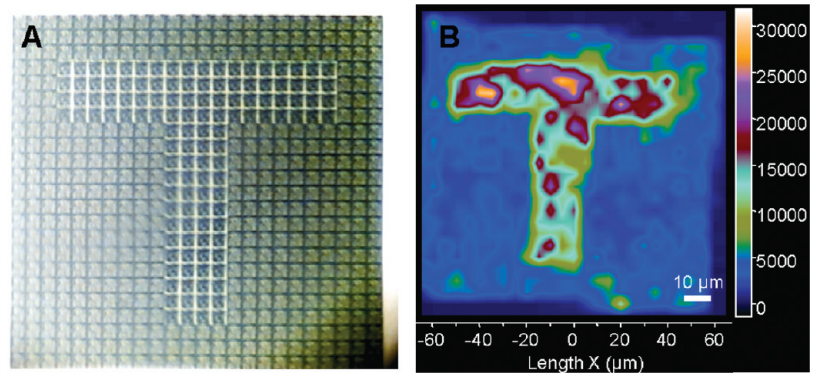

Figure 4. Demonstrated ability to clone hot cells into macropatterns. (A) An image from an optical microscope where the inner "T" is a cloned cell from a high performing cell and the outside is from a modest performing cell. (B) Map showing uniform enhancement from both the outer and inner regions.

It has been shown in previous work involving single molecule SERS (SMSERS)[38−40] that electromagnetic EF can approach 10^{11}. While of great significance in SMSERS, these active hot spots with exceptional EF represent only a minuscule percentage of the total substrate area. When comparing the enhancement of a single molecule, it has been shown that the enhancement can be as much as 10^7 times greater than the average enhancement of the entire substrate.[19] From a trace analysis standpoint, this can be a significant analysis limitation as the trace analyte must find the appropriate spot of the substrate. In our approach, however, we were able to produce an enhancement of 5×10^8 for a large area metal surface. Although Figure 3C clearly indicates the enhancement is not uniform over the entire LDNA metal surface, it is observed that when moving the interrogation laser spot over the entire substrate the average enhancement does not deviate appreciably (RSD of ~30%). While we do not demonstrate a single aggregate with enhancement approaching theoretical limits, it is possible to create a substrate with high enhancement over relatively large areas (hot cells can be cloned at a rate of roughly 0.1 mm^2/min with our system).

Analytical Figures of Merit with Cloned LDNAs. The benefits of a large substrate area also extend into an ability to improve on many figures of merit including reproducibility. One method for improving is altering the way the substrate is analyzed. When laser exposure is increased, the potential for larger signal and better sensitivity increases. However, one issue that can arise is sample photodegradation and substrate damage when a large laser power is used.[41,42] One way our group has addressed this problem involves using a sample translation technique (STT) wherein the analyte baring substrate is spun under the focused laser beam to reduce the effective duty cycle of irradiation.[42] As such, the ability to use higher powers and long acquisition times without damaging the sample or the substrate leads to improved limits of detection and sensitivity. Moreover, inhomogeneity in the substrate is averaged out with the STT approach.[42] Large area cloned LDNAs and the STT appear to be a well-suited match.

Using the same cells as used in the inner part of the cloned T array, a large 300×900 μm array was created. For these experiments, the usual settings of a 1 s acquisition with a laser power of 0.67 mW were altered to accommodate harsher conditions. Using this large region, STT was used to analyze the substrate. Translation of the sample was achieved by spinning the substrate at a rate of approximately 2000 rpm and optically interrogating. While spinning, the average signal of each concentric ring was acquired. This process allows the acquisition time to increase without damaging the substrate or degrading the analyte in the process. Using 5×10^{-7} M rhodamine 6G (R6G), a comparison of the reproducibility of STT and a stationary substrate using a 10 s acquisition time at the 0.67 mW power was investigated. As seen in Figure 5A, the spectra for the STT analyses were not only similar but they also produced an RSD of 6.6% for the 1499 cm^{-1} band. The stationary acquisition, however, produced an RSD value of 22% on this substrate for the same band. While the stationary raster approach is fairly reproducible as far as SERS analysis goes, using the STT allows excellent reproducibility.

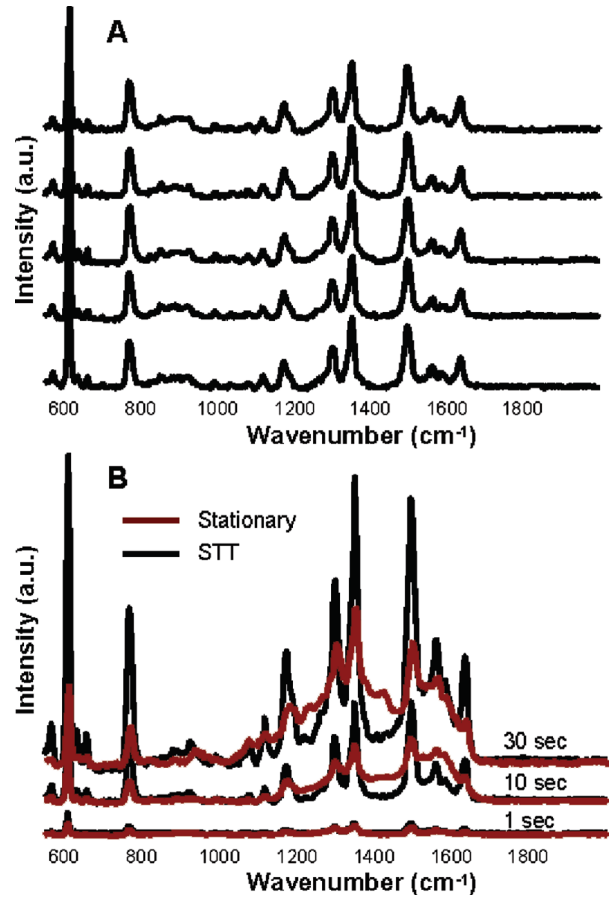

Figure 5. (A) Comparison of spectra for R6G during one trial of extended regions of cloned cells and employing STT with incremental increases in spinning radius of about 5 μm each for the spectra and demonstrating very good reproducibility. (B) Spectra indicating the analytical improvement in S/N by virtue of using the STT approach, over single point measurements, by increasing acquisition times with R6G as the analyte.

The large substrate allows for much harsher conditions than would be possible using SMSERS experimental protocols. The same cloned arrays were exposed to a laser power of 2.7 mW. Using both the STT and a stationary raster, 5×10^{-7} M R6G was analyzed with various acquisition times ranging from 1 to 30 s. As seen in Figure 5B, there is a large difference between the spectra of the STT and stationary acquisitions. Initially, the 1 s acquisition time for each technique is strikingly similar. However, when using a 10 s acquisition time, the in-

tensity for the STT starts to outpace the stationary technique. Also, some of the bands start to show signs of degradation with concomitant carbonation formation (see broad region from 1000 to 1600 cm^{-1}).[42] By the time the 30 s acquisition times are used, the difference between techniques is even more pronounced, with many STT bands subsequently more intense than those of the stationary raster. Also, the broad carbonation bands with the stationary raster have obscured the R6G bands almost completely while the STT spectrum is still distinct. Large area LDNAs substrates, therefore, have the ability to withstand harsh conditions without degrading due to the potential of alternate analysis techniques. This is expected to translate into improved calibration plots with lower limits of detection. These improvements correlate to an average signal intensity height of 13 375 at the 602 cm^{-1} band with a 30 s acquisition time using the STT, more than 28 times better than the 1 s stationary raster.

CONCLUSIONS

In summary, while colloidal deposition can achieve individual aggregates with large SERS enhancement, the ability of EBL to reproducibly fabricate high performing pseudoaggregates makes it an attractive approach for substrate creation. Moreover, through the use of EBL, we were able to consistently identify the "hot" regions (cells) on multiple fabrication attempts. Through a combinatorial-like, spectral mapping approach to hot cell identification, it was possible to not only locate an individual cell capable of high signal intensity but also to dissect the individual cells to further study morphological features leading to SERS enhancement. Using the cells denoted as the best performing, we are able to clone large arrays that yielded electromagnetic enhancement of 5×10^8 with good uniformity, providing improved analytical capabilities by mating with STT. While more straightforwardly created, nonlithographic substrates such as metal films over nanospheres can achieve enhancements of 1×10^8 over relatively large areas,[44,45] we contend that by dissecting cells more acutely (as see in Figure 3), and/or exploring additional nanoparticle shapes and sizes, extended LDNA surfaces may be fabricated with uniform enhancements significantly better than the 5×10^8 reported herein.

MATERIALS AND METHODS

Instrumentation. All SERS spectra were collected using a JY-Horiba LabRam Spectrograph. Details of the instrument setup have been described previously.[42,46] In general, a 50× (0.45 NA, ∞) microscope objective was used to deliver 0.67 mW of the 633 nm line of a thermoelectrically cooled HeNe laser with a spot size of approximately 5 μm. All spectra were collected with a 180° scattering geometry, and sample acquisition times were set to 1 s unless otherwise stated. The polarization vector was vertical in the plane of the substrate arrays in all cases. Normally, SERS spectra are manually corrected for the broad background scatter using the LabSpec 4.12 software of our Raman system.

Preparation of SERS-Active Substrates. As described above, 50 × 50 μm patterns containing different shapes of varying sizes (see appearance in Figure 1A), randomly positioned in the array to form 5 × 5 μm cells, were created in AutoCAD 2005. These arrays were formed with either various shapes or different circles and ellipses to create the pattern types seen in Table 1. The patterns were each created by selecting the types of shapes as well as the sizes to use for that pattern. Subsequently, individual shapes were manually inserted into a 50 × 50 μm CAD square in a random, blind fashion until a predetermined overall average density (percent coverage/5 × 5 μm cell) was reached. Some manipulation of the CAD patterns was performed so that the larger CAD square was partitioned into 100 smaller 5 × 5 μm cells that roughly match the laser spot size.

Once a strong performing hot cell was pin-pointed *via* SERS data collection (described below), that 5 × 5 μm cell was found in the original AutoCAD drawing and cloned into a macropattern in the shape of a T (called "cloned cell 'T' pattern"). The AutoCAD drawings were then converted to GDS-II format by using the LinkCAD conversion program. The files were transferred to the EBL system computer and converted to the format readable by the instrument.

Liftoff Pillar Method: A 2 in. Si wafer (Wafer World, FL) was baked for 45 min at 250 °C to remove any excess moisture adsorbed onto the surface. A 300 nm film of Zep 520A, a high-resolution positive tone resist suspended in anisole, was applied to the wafer using spin coating at 6000 rpm for 45 s. Once coated, the wafer was then baked at 180 °C for 2 min and placed under vacuum in the EBL system. The resist film thickness was estimated from a chart provided by the manufacturer based on spin rate.

A Jeol JBX-9300 FS/E EBL system with a 100 keV thermal field emission gun was used for the writing of the nanoarrays. The resist film was exposed to a dose of 420 $\mu C/cm^2$ for fabrication. Each 50 × 50 μm pattern was spaced 200 μm apart in both the *x* and *y* directions, yielding evenly spaced rows of unique patterns. Each row has similar features, while each column has varied individual patterns. When exposure was complete, the patterns were developed using xylene for 30 s, rinsed with isopropyl alcohol, and dried. Wafers were then exposed to an O_2 plasma for 6 s at 100 W (Technics Reactive Ion Etching System) to remove resist residue on the patterns after development.

For the liftoff process, 10 nm of chromium was then deposited onto the surface of the wafer using an electron-beam dual gun evaporation chamber (Thermonics Laboratory, VE- 240). The excess resist and chromium were then removed *via* liftoff using an acetone bath followed by an isopropyl alcohol rinse. The wafers are then rinsed with deionized water and dried. The patterns were then etched using an Oxford RIE to a pillar height of 250 nm at a rate of 100 nm/min (see appearance in Figure 1B). After etching, the chromium was removed using a chromium photomask etchant, Cr-14S, bath for 20 min. Finally, 20 nm of SiO_2 was deposited onto the silicon surface using an Oxford Plasma Enhanced Chemical Vapor Deposition system at a rate of 1.2 nm/s (see appearance in Figure 1C).

Substrates were made SERS-active by deposition of 99.999% Ag (Alfa Aesar, MA) using a physical vapor deposition (PVD) chamber from Cooke Vacuum Products, Inc. Samples were mounted 25 cm above and normal to the effusive source. Average mass thickness and deposition rates were monitored for each film using a quartz-crystal microbalance (QCM) mounted adjacent to the substrates. The SiO_2 patterns were coated with varying amounts of Ag at differing deposition rates depending on the study being done (see appearance in Figure 1D).

Scanning electron microscopy (SEM) images were collected with a Jeol JSM-7400F microscope with a field emission gun operating at a range of 1.50−5.00 kV depending on the substrate surface. Sample damage and charge buildup were reduced under these conditions to yield high-resolution images of Ag-coated and uncoated surfaces.

Analyte Preparation and Data Acquisition. The analyte used in most studies was 1×10^{-5} M benzenethiol (99%, Fisher) in 18 MΩ deionized water (Barnstead, E-Pure), which formed a well-defined SAM on the metal surface. Details of how data was collected and processed have been described previously.[42,43] The wafer containing the rows of patterns was placed at the bottom of a plastic Petri dish that was filled with approximately 2 mL of BT solution for 15 min before being rinsed with deionized water and dried. SERS signal was optimized by fine-focusing the microscope objective, and the spectroscopic data were collected by rastering the laser beam across each pattern at 5 μm intervals (1 spectral acquisition per step) over a 4900 μm^2 area ($N = 196$). In some studies, a previously described STT[42,46] was used, while other test analytes were sometimes used, as well. It should be noted that the laser spot jitter on our nanofabricated samples is estimated to be 1−2 μm and was influenced by construction near our laboratory.

Acknowledgment. This research was supported by the U.S. Environmental Protection Agency STAR Program under Grant EPA-83274001 with the University of Tennessee. The nanofabrication portion of this research, conducted at Oak Ridge National Laboratory's Center for Nanophase Materials Sciences, was sponsored by the Scientific User Facilities Division, Office of Basic Energy Sciences, U.S. Department of Energy.

REFERENCES AND NOTES

1. Moskovits, M. Surface-Enhanced Spectroscopy. *Rev. Mod. Phys.* **1985**, *57*, 783–826.
2. Otto, A. *Light Scattering in Solids*; Springer: Berlin, 1984.
3. Otto, A.; Mrozek, I.; Grabhorn, H.; Akemann, W. Surface-Enhanced Raman Scattering. *Phys. Chem.: Condens. Matter.* **1992**, *4*, 1143–1212.
4. Garcia-Vidal, F. J.; Pendry, J. B. Collective Theory for Surface Enhanced Raman Scattering. *Phys. Rev. Lett.* **1996**, *77*, 1163–1166.
5. Vo-Dinh, T.; Bello, J. M. Surface-Enhanced Raman Scattering Fiber-Optic Sensor. *Appl. Spectrosc.* **1990**, *44*, 63–69.
6. Wokaun, A. Surface-Enhanced Electromagnetic Processes. *Solid State Phys.* **1984**, *38*, 223–294.
7. Ritchie, R. H. Plasma Losses by Fast Electrons in Thin Films. *Phys. Rev.* **1957**, *106*, 874–881.
8. Kneipp, K.; Wang, Y.; Kneipp, H.; Perelman, L. T.; Itzkan, I.; Dasari, R. R.; Feld, M. S. Single Molecule Detection Using Surface-Enhanced Raman Scattering. *Phys. Rev. Lett.* **1997**, *78*, 1667–1670.
9. Kelly, K. L.; Coronado, E.; Zhao, L. L.; Schatz, G. C. The Optical Properties of Metal Nanoparticles: The Influence of Size, Shape, and Dielectric Environment. *J. Phys. Chem. B* **2003**, *107*, 668–677.
10. Oubre, C.; Nordlander, P. Finite-Difference Time-Domain Studies of the Optical Properties of Nanoshell Dimers. *J. Phys. Chem. B* **2005**, *109*, 10042–10051.
11. Green, M.; Liu, F. M. SERS Substrates Fabricated by Island Lithography: The Silver/Pyridine System. *J. Phys. Chem. B* **2003**, *107*, 13015–13021.
12. Kaminska, A.; Inya-Agha, O.; Forster, R. J.; Keyes, T. E. Chemically Bound Gold Nanoparticle Arrays on Silicon: Assembly, Properties, and SERS Study of Protein Interaction. *Phys. Chem. Chem. Phys.* **2008**, *10*, 4172–4180.
13. Yan, B.; Thubagere, A.; Premasiri, W. R.; Ziegler, L. D.; Dal Negro, L.; Reinhard, B. M. Engineered SERS Substrates with Multiscale Signal Enhancement: Nanoparticle Cluser Arrays. *ACS Nano* **2009**, *3*, 1190–1202.
14. Kneipp, K.; Kneipp, H.; Itzkan, I.; Dasari, R. R.; Feld, M. S. Ultrasensitive Chemical Analysis by Raman Spectroscopy. *Chem. Rev.* **1999**, *99*, 2957–2975.
15. Emory, S. R.; Nie, S. Near-Field Surface-Enhanced Raman Spectroscopy on Single Silver Nanoparticles. *Anal. Chem.* **1997**, *69*, 2631–2635.
16. Aroca, R. F.; Alvarez-Puebla, R. A. Raman Scattering on Colloidal Nanostructures. *Adv. Colloid Interface Sci.* **2005**, *116*, 45–61.
17. Khan, I.; Cunninghan, D.; Graham, D.; McComb, D. W.; Smith, W. E. Identification and Characterization of Active and Inactive Species for Surface-Enhanced Resonance Raman Scattering. *J. Phys. Chem. B* **2005**, *109*, 3454–3459.
18. Michaels, A. M.; Nirmal, M.; Brus, L. E. Surface Enhanced Raman Spectroscopy of Individual Rhodamine 6G Molecules on Large Ag Nanocrystals. *J. Am. Chem. Soc.* **1999**, *121*, 9932–9939.
19. Nie, S.; Emory, S. R. Probing Single Molecules and Single Nanoparticles by Surface-Enhanced Raman Scattering. *Science* **1997**, *275*, 102–106.
20. Michaels, A. M.; Jiang, J.; Brus, L. E. Ag Nanocrystal Junctions as the Site for Surface-Enhanced Raman Scattering of Single Rhodamine 6G Molecules. *J. Phys. Chem. B* **2000**, *104*, 11965–11971.
21. Markel, V. A.; Shalev, V. M.; Zhnag, P.; Huynh, W.; Tay, L.; Haslet, T. L.; Moscovits, M. Near-Field Optical Spectroscopy of Individual Surface-Plasmon Modes in Colloid Clusters. *Phys. Rev. B* **1999**, *59*, 10903–10909.
22. Camden, J. P.; Dieringer, J. A.; Wang, Y.; Masiello, D. J.; Marks, L. D.; Schatz, G. C.; Van Duyne, R. P. Probing the Structure of Single-Molecule Surface-Enhanced Raman Scattering Hot Spots. *J. Am. Chem. Soc.* **2008**, *130*, 12616–12617.
23. Li, H.; Cullum, B. M. Dual Layer and Multilayer Enhancements from Silver Film over Nanostructured Surface-Enhanced Raman Substrates. *Appl. Spectrosc.* **2005**, *59*, 410–417.
24. De Jesus, M. A.; Giesfeldt, K. S.; Oran, J. M.; Abu Hatab, N. A.; Lavrik, N. V.; Sepaniak, M. J. Nanofabrication of Densely Packed Metal-Polymer Arrays for Surface-Enhanced Raman Spectrometry. *Appl. Spectrosc.* **2005**, *59*, 1501–1508.
25. Abu Hatab, N. A.; Oran, J. M.; Sepaniak, M. J. Surface-Enhanced Raman Spectroscopy Substrates Created *via* Electron Beam Lithography and Nanotransfer Printing. *ACS Nano* **2008**, *2*, 377–385.
26. Oran, J. M.; Hinde, R. J.; Abu Hatab, N.; Retterer, S. T.; Sepaniak, M. J. Nanofabricated Periodic Arrays of Silver Elliptical Disks as SERS Substrates. *J. Raman Spectrosc.* **2008**, *39*, 1811–1820.
27. Alexander, T. A.; Wickenden, A. E. Electron-Beam-Lithography (EBL)-Engineered Nanostructures for Biosensing. Proceedings of SPIE-The International Society for Optical Engineering; Philadelphia, PA, October 24, 2004; Cullum, B. M., Ed.; SPIE: Bellingham, WA, 2004; pp 78−86.
28. Abu Hatab, N. A.; John, J. F.; Oran, J. M.; Sepaniak, M. J. Multiplexed Microfluidic Surface-Enhanced Raman Spectroscopy. *Appl. Spectrosc.* **2007**, *61*, 1116–1122.
29. Schoenfischm, M. H.; Pemberton, J. E. Air Stability of Alkanethiol Self-Assembled Monolayers on Silver and Gold Surfaces. *J. Am. Chem. Soc.* **1998**, *120*, 4502–4513.
30. Han, S. W.; Lee, S. J.; Kim, K. Self-Assembled Monolayers of Aromatic Thiol and Selenol on Silver: Comparative Study of Adsorptivity and Stability. *Langmuir* **2001**, *17*, 6981–6987.
31. Bijeon, J. L.; Royer, P.; Goudonnet, J. P.; Warmack, R. J.; Ferrell, T. L. Effects of a Silicon Substrate on Surface Plasmon Spectra in Silver Island Films. *Thin Solid Films* **1987**, *155*, L1–L3.
32. Daniels, J. K.; Chumanov, G. Nanoparticle-Mirror Sandwich Substrates for Surface-Enhanced Raman Scattering. *J. Phys. Chem. B* **2005**, *109*, 17936–17942.
33. Kinnan, M. K.; Chumanov, G. Surface Enhanced Raman Scattering from Silver Nanoparticle Arrays on Silver Mirror Films: Plasmon-Induced Electronic Coupling as the Enhancement Mechanism. *J. Phys. Chem. C* **2007**, *111*, 18010–18017.
34. Le Ru, E. C.; Blackie, E.; Meyer, M.; Etchegoin, P. G. Surface Enhanced Raman Scattering Enhancement Factors: A Comprehensive Study. *J. Phys. Chem. C* **2007**, *111*, 13794–13803.

35. Haynes, C. L.; Van Duyne, R. P. Plasmon-Sampled Surface-Enhanced Raman Excitation Spectroscopy. *J. Phys. Chem. B* **2003**, *107*, 7426–7433.
36. Wan, L.-J.; Terashima, M.; Noda, H.; Osawa, M. J. Molecular Orientation and Ordered Structure of Benzenethiol Adsorbed onto Gold. *Phys. Chem. B* **2000**, *104*, 3563–3569.
37. Whelan, C. M.; Smyth, M. R.; Barnes, C. J. HREELS, XPS, and Electrochemical Study of Benzenethiol Adsorption on Au(111). *Langmuir* **1999**, *15*, 116–126.
38. Xu, H.; Aizpurua, J.; Käll, M.; Apell, P. Electromagnetic Contributions to Single-Molecule Seneitivity in Surface-Enhanced Raman Scattering. *Phys. Rev. E* **2000**, *62*, 4318–4324.
39. Xu, H. X.; Bjerneld, E. J.; Kall, M.; Borjesson, L. Surface-Enhanced Raman Scattering on Silver Nanoparticles in Different Aggregation Stages. *Phys. Rev. Lett.* **1999**, *83*, 4357–4360.
40. Li, K. R.; Li, X. T.; Stockman, M. I.; Bergman, D. J. Surface Plasmon Amplification by Stimulated Emission in Nanolenses. *Phys. Rev. B* **2005**, *71*, 115409/1–115409/5.
41. Khan, I.; Powlwart, E.; McComb, D. W.; Smith, W. E. Correlation of Optical Properties with Structure of Immobilized Nanoparticles—A Method for Probing the Mechanism of SERRS. *Analyst* **2004**, *129*, 950–955.
42. De Jesus, M. A.; Giesfeldt, K. S.; Sepaniak, M. J. Use of Sample Translation Technique to Minimize Adverse Effects of Laser Iirradiation in Surface-Enhanced Raman Spectrometry. *Appl. Spectrosc.* **2003**, *57*, 428–438.
43. Giesfeldt, K. S.; Connatser, R. M.; DeJesus, M. A.; Lavrik, N. V.; Dutta, P.; Sepaniak, M. J. Studies of the Optical Properties of Metal-Pliable Polymer Composite Materials. *Appl. Spectrosc.* **2003**, *57*, 1346–1352.
44. McFarland, A. D.; Young, M. A.; Dieringer, J. A.; Van Duyne, R. P. Wavelength-Scanned Surface-Enhanced Raman Excitation Spectroscopy. *J. Phys. Chem. B* **2005**, *109*, 11279–11285.
45. Dick, L. A.; McFarland, A. D.; Haynes, C. L.; Van Duyne, R. P. Metal Films over Nanosphere (MFON) for Surface-Enhanced Raman Spectroscopy (SERS): Improvements in Surface Nanostructure Stability and Suppression of Irreversible Loss. *J. Phys. Chem. B* **2002**, *106*, 853–860.
46. Bhandari, D.; Walworth, M. J.; Sepaniak, M. J. Dual Function Surface-Enhanced Raman Active Extractor for the Detection of Environmental Contaminants. *Appl. Spectrosc.* **2009**, *63*, 571–578.